The torso surface can be represented by any complete set of orthogonal functions, such as Fourier functions. However, unlike the 2- and 3-D Fourier representations [20], [21], the surface harmonic expansion method can reconstruct the boundary shapes from an arbitrary set of measured boundary points, regardless of their placement and ordering. In addition, compared to the interpolation techniques [22], the boundary is described by the sum of known functions in a simple and continuous form. Recently, Nielsen *et al.* [23] presented an efficient way for reconstruction of the heart surfaces. This description can also be extended to realistic torso models. Although their method is an important contribution to realistic modeling techniques, it is highly labor-intensive [23].

ACKNOWLEDGMENT

The authors wish to thank D. Vardy for digitizing the torso models and A. S. Ferguson and S. Ritcey for careful reading of the manuscript.

REFERENCES

[1] M. D. Altschuler, M. R. Sontag, and B. Peters, "A clinically operational method for three-dimensional dose calculations," *Phys. Med. Biol.*, vol. 30, pp. 217–228, 1985.
[2] A. Niemierko and M. Goitein, "The use of variable grid spacing to accelerate dose calculation," *Med. Phys.*, vol. 16, pp. 357–366, 1989.
[3] R. M. Gulrajani, F. A. Roberge, and G. E. Mailloux, "The forward problem of electrocardiography," in *Comprehensive Electrocardiology*, P. W. Macfarlane and T. D. Veitch-Lawrie, Eds. New York: Pergamon, 1989, pp. 197–236.
[4] R. M. Gulrajani, P. Savard, and F. A. Roberge, "The inverse problem in electrocardiography: Solution in terms of equivalent sources," *CRC Crit. Rev. Biomed. Eng.*, vol. 16, pp. 171–214, 1988.
[5] G. Stroink, "Cardiomagnetic imaging," in *Frontiers in Cardiovascular Research*, B. L. Zaret, L. Kaufman, S. Berson, and R. A. Dunn, Eds. New York: Raven, 1993, pp. 161–177.
[6] B. M. Horáček, "Numerical models of an inhomogeneous human torso," *Adv. Cardiol.*, vol. 10, pp. 51–57, 1974.
[7] Y. Rudy and B. J. Messinger-Rapport, "The inverse solution in electrocardiography: Solutions in terms of epicardial potentials," *CRC Crit. Rev. Biomed. Eng.*, vol. 16, pp. 215–268, 1988.
[8] C. J. Purcell, G. Stroink, and B. M. Horáček, "Effect of torso boundaries on electric potential and magnetic field of a dipole," *IEEE Trans. Biomed. Eng.*, vol. 35, pp. 671–677, 1988.
[9] P. C. Stanley, T. C. Pilkington, and M. N. Morrow, "The effect of thoracic inhomogeneities on the relationship between epicardial and torso potentials," *IEEE Trans. Biomed. Eng.*, vol. BME-33, pp. 273–284, 1986.
[10] G. J. Huiskamp and A. Van Oosterom, "Tailored versus realistic geometry in the inverse problem of electrocardiography," *IEEE Trans. Biomed. Eng.*, vol. 36, pp. 827–835, 1989.
[11] R. Hren, "The effect of inhomogeneities on electrocardiographic and magnetocardiographic inverse solutions: Application in the localization of ventricular pre-excitation sites," M.Sc. thesis, Dalhousie University, Nova Scotia, Canada, 1993.
[12] C. J. Purcell, T. Mashiko, K. Odaka, and K. Ueno, "Describing head shape with surface harmonic expansions," *IEEE Trans. Biomed. Eng.*, vol. 38, pp. 303–306, 1991.
[13] O. D. Kellog, *Potential Theory*. Berlin: Springer-Verlag, 1929.
[14] W. J. Sternberg and T. L. Smith, *The Theory of Potential and Spherical Harmonics*. Toronto: Toronto University Press, 1948.
[15] T. M. MacRobert, *Spherical Harmonics—An Elementary Treatise on Harmonic Functions with Applications*. New York: Pergamon, 1967.
[16] W. H. Press, B. P. Flannery, S. A. Teukolsky, and W. T. Vetterling, *Numerical Recipes—The Art of Scientific Computing*. Cambridge, MA: Cambridge University Press, 1992.
[17] X. Zhang and G. Stroink, "A node-based boundary element method to calculate the continuous variations of cardiac potential over a closed surface," in *Proc. Annu. Int. Conf. IEEE EMBS*, J. P. Morucci, R. Plonsey, J. L. Coatrieux, and S. Laxminarayan, Eds. Paris: IEEE Press, 1992, pp. 1770–1771.
[18] J. Lant, G. Stroink, B. ten Voorde, B. M. Horáček, and T. J. Montague, "Complementary nature of electrocardiographic and magnetocardiographic data in patients with ischemic heart disease," *J. Electrocardiol.*, vol. 23, pp. 315–321, 1990.
[19] R. C. Barr, T. M. Gallie, and M. S. Spach, "Automated production of contour maps for electrophysiology II. Triangulation, verification and organization of the geometric model," *Comput. Biomed. Res.*, vol. 13, pp. 154–170, 1980.
[20] A. Van Oosterom, "Triangulating the human torso," *Comput. J.*, vol. 21, pp. 253–258, 1977.
[21] K. S. Park and N. S. Lee, "A three-dimensional Fourier descriptor for human body representation/reconstruction from serial cross sections," *Comput. Biomed. Res.*, vol. 20, pp. 125–140, 1987.
[22] W. Lin, S. Cheng, and C. Chen, "A new surface interpolation technique for reconstructing 3-D objects from serial cross-sections," *Comput. Vision Graphics Image Processing*, vol. 48, pp. 124–143, 1989.
[23] P. M. F. Nielsen, I. J. Le Grice, B. H. Smaill, and P. J. Hunter, "Mathematical model of geometry and fibrous structure of the heart," *Amer. J. Physiol.*, vol. 260, pp. H1365–H1378, 1991.

Data Transmission from an Implantable Biotelemeter by Load-Shift Keying Using Circuit Configuration Modulator

Zhengnian Tang, Brian Smith, John H. Schild, and P. Hunter Peckham

***Abstract*—Using the reflected impedance property of an inductive couple (transformer), a modulation method, Load-Shift Keying using Circuit Configuration Modulator (LSK-CCM), was developed to perform data transmission from an implantable telemeter. With a very simple circuit, this method utilizes a radio-frequency electromagnetic field induced with a single pair of coils to transmit power into the implant and data out of it.**

I. INTRODUCTION

For over forty years, implantable telemetry systems have been used for animal experiments and human applications, including measurements of heart rate, ECG, EEG, temperature, pH, and pressure and prosthesis purposes [1], [5], [7], [10], [12], [17], [18]. Most implantable telemeters use frequency modulation (FM) for signal transmission [2], [5], [7]–[9], [12]. In closely coupled telemetry, FM signal recovery is not affected by the continuous relative movement between transmitting and receiving antennas. This makes FM the practical choice for analog signal transmission. To transmit digital signal, however, several modulation schemes can be used, including amplitude-shift keying (ASK), frequency-shift keying (FSK), and phase-shift keying (PSK). ASK uses the simplest modulation circuit such that the implanted circuit complexity is minimized [13], [17]. With proper design ensuring acceptable modulation index and signal-

Manuscript received July 2, 1993; revised January 25, 1995. This work was supported by Grant NS29549 from the National Institutes of Health—National Institute on Neurological Diseases and Stroke.

Z. Tang is with the Department of Biomedical Engineering, Case Western Reserve University, Cleveland, OH 44106 USA.
B. Smith and P. H. Peckham are with the Rehabilitation Engineering Center, Case Western Reserve University and Cleveland FES Center, Cleveland, OH 44106 USA.
J. H. Schild is with the Department of Molecular Physiology and Biophysics, Baylor College of Medicine, Waco, TX 76703 USA.

IEEE Log Number 9410027.

to-noise ratio (SNR), the quality of the digital data transmission using ASK will be more than sufficient in many applications.

As part of an advanced functional electrical stimulation (FES) system, an implantable telemeter was developed for transmitting four channels of electromyographic (EMG) data acquired with implanted electrodes [13], [15]. The telemeter conditions, samples, and digitizes acquired signals using binary pulse-code modulation (PCM), which allows accurate data coding and transmission with a relatively simple circuit. The digitized signal being transmitted is serial binary data at 36 kb/s. A 300-kHz square wave synchronization burst is placed at the beginning of each channel 1–4 sequence for external decoding purposes. Continuous operation of the implanted electronic circuit requires 80 mW of dc power [13], which requires that the implant be powered externally through a high-efficiency transcutaneous radio frequency (RF) couple.

Load-shift keying (LSK), which was referred as "reflectance modulation" [13], [15], is a communication scheme which allows simultaneous powering and data transmission through the same RF inductive couple. It is a particular form of ASK. The RF power link is basically a transformer formed with two flat inductive coils. LSK utilizes the property of an inductive couple in which a change of the secondary load is reflected onto the primary coil as a varying impedance (i.e., reflected impedance). The modulation circuitry is implemented by using a "circuit configuration modulator (CCM)," a novel switch circuitry developed to realize LSK. CCM uses a simple circuit to make the acquired and digitized data modulate the effective secondary power recovery circuit configuration, and hence the effective secondary load reflected onto the primary coil. With proper RF coil design, reliable data transmission can be achieved by using LSK-CCM without significantly altering power transmission efficiency.

II. Theoretical Basis

A. Load-Shift Keying, LSK

One common way of achieving ASK through an inductive couple consisting of a pair of RF coils is to modulate resonant capacitance or coil inductance of the secondary (power receiving) circuit. The resultant shifts in resonant frequency are reflected back upon the external coil as changes in the voltage amplitude across it [17]. By monitoring and decoding the voltage waveform across the external coil, the data are recovered. However, when the communications link is incorporated into an RF powering link, this approach may lead to significant power efficiency decrease. Therefore, an alternative method was sought.

An inductive couple has the property that changes in the loading of the secondary coil are reflected back as changes in the loading of the primary coil. This provides a possible means of implementing ASK. Consider the circuit configuration shown in Fig. 1, Z_r is the reflected impedance which appears as part of the total impedance of the primary coil [16]

$$Z_r = \frac{(\omega M)^2}{Z_2}. \tag{1}$$

where Z_2 is the load impedance seen by the secondary coil, ω is the angular frequency of the RF power carrier, and M is the mutual inductance between the primary and the secondary coils. The impedance of the primary circuit is

$$Z_1 = \frac{V_1}{I_1} = R_1 + Z_r + j\left[\omega L_1 - \left(\frac{1}{\omega C_1}\right)\right]. \tag{2}$$

Considering the secondary coil L_2 as a dependent voltage source V_2 in series with impedance $j\omega L_2$, the load impedance on the secondary

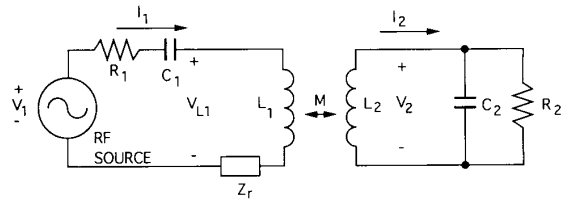

Fig. 1. The circuit for the analysis of LSK principle. Z_r and L_1 constitute the model for the primary coil. (Primary is on the left, secondary on the right.)

coil is

$$Z_2 = \frac{V_2}{I_2} = j\omega L_2 + \left(\frac{1}{R_2} + j\omega C_2\right)^{-1} = \frac{R_2}{1+\omega^2 R_2^2 C_2^2} + j\left(\omega L_2 - \frac{\omega C_2 R_2^2}{1+\omega^2 R_2^2 C_2^2}\right). \tag{3}$$

Both primary and secondary circuits operate at a common resonant frequency ω, so Z_1 and Z_2 are purely resistive. Thus, in (2) and (3),

$$j\left(\omega L_1 - \frac{1}{\omega C_1}\right) = 0 \tag{4}$$

and

$$j\left(\omega L_2 - \frac{\omega C_2 R_2^2}{1+\omega^2 R_2^2 C_2^2}\right) = 0. \tag{5}$$

Rearranging (5) gives

$$\frac{1}{1+\omega^2 R_2^2 C_2^2} = \frac{L_2}{C_2 R_2^2}. \tag{6}$$

which is substituted into (3) to get

$$Z_2 = \frac{R_2}{1+\omega^2 R_2^2 C_2^2} = \frac{L_2}{R_2 C_2}. \tag{7}$$

The definition of mutual inductance is given by

$$M = k(L_1 L_2)^{1/2}. \tag{8}$$

where k is the coupling coefficient defined by geometrical parameters [16]. By combining (1) and (4)–(8), we obtain

$$Z_1 = R_1 + \omega^2 k^2 L_1 C_2 R_2. \tag{9}$$

Defining V_{L1} as the voltage across the primary coil, then

$$V_{L1} = \left(\frac{\omega L_1}{Z_1}\right) V_1 = \left(\frac{1}{\omega C_1 Z_1}\right) V_1. \tag{10}$$

Substituting Z_1 by the term given as (9), we have

$$V_{L1} = \frac{V_1}{\omega C_1 (R_1 + \omega^2 k^2 L_1 C_2 R_2)}. \tag{11}$$

If the secondary resistive load changes from R_2 to R_2', then

$$V_{L1}' = \frac{V_1}{\omega C_1 (R_1 + \omega^2 k^2 L_1 C_2 R_2')}. \tag{12}$$

The modulation index, which is the ratio of signal amplitude to carrier amplitude in amplitude modulation (AM) and also referred as percentage of modulation, is then

$$m = \left|\frac{V_{L1} - V_{L1}'}{V_{L1} + V_{L1}'}\right|. \tag{13}$$

This analysis has been experimentally verified by adding a data-driven voltage-controlled resistor in parallel with the original load R_2 and examining the voltage across the primary coil. In practice, however, shunting resistance to the secondary load leads to significant loss of energy.

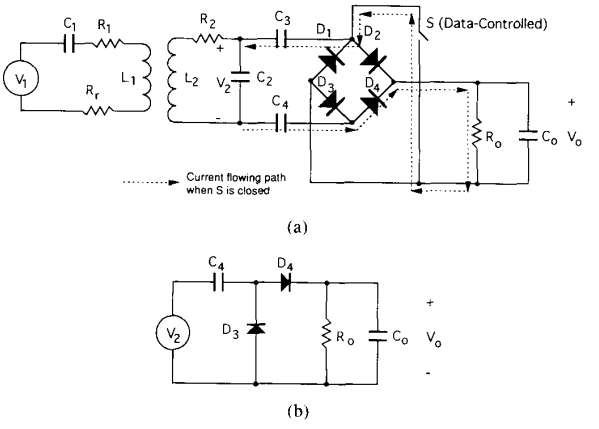

Fig. 2. An illustration of how CCM operates. (a) The CCM circuit. When the switch is open, the power recovery circuit is a full-wave rectifier. (Primary is on the left, secondary on the right.) (b) The equivalent circuit when the switch is closed, which is a voltage clamp (secondary).

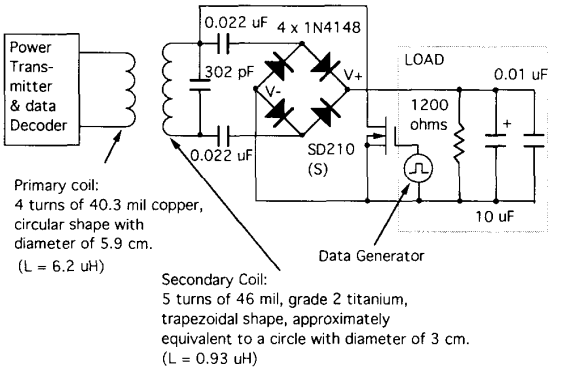

Fig. 3. The illustration of the RF powering and communications system constructed to evaluate LSK-CCM, with the actual component parameters marked. The operating frequency is 8.75 MHz, at which both primary and secondary circuits resonate.

B. Circuit Configuration Modulator, CCM

The realization of LSK needs a physically simple circuit to modulate the secondary load with digital data while maintaining adequate RF power transmission efficiency. In an RF powering circuit, the effective ac load applied onto the secondary coil is a function of both the dc load and the configuration of the RF power recovery circuit. Modulating the configuration of the secondary power receiving circuitry provides an alternative to modulating the dc load with a shunt resistor. That is, a data-driven switch enables one circuit configuration when the data bit is "0" and the other when the data bit is "1." The two circuit configurations need to provide very different ac loads but similar power efficiency.

Fig. 2(a) shows the basic CCM circuit. In this circuit, R_o is the dc load resistance, C_o is the dc load capacitance, and f is the operating frequency of the RF power link. $R_oC_o \gg 1/2\pi f$, such that C_o can be neglected in the circuit analysis. The peak ac voltage across the secondary tank circuit L_2C_2, V_{2pk} is much larger than the voltage drop across the diodes D_1–D_4 such that $V_{2pk} \approx V_o$. When S is open, the circuit is a full-wave rectifier. The equivalent ac load resistance R_{ac}, which will dissipate an amount of power equivalent to the dc

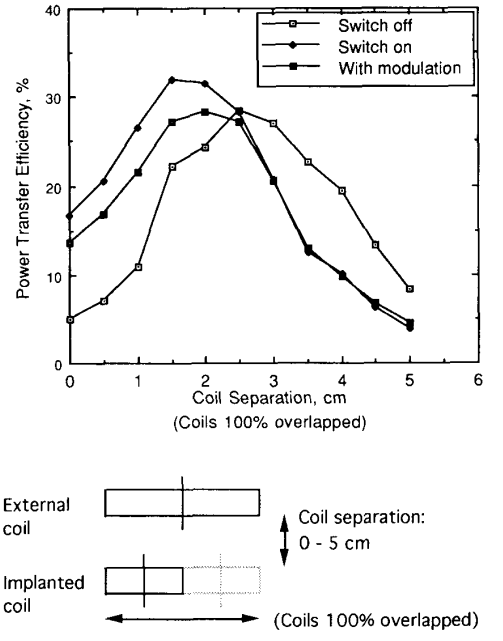

Fig. 4. Power transfer efficiency versus coil separation, measured with the circuit in Fig. 4. Modulation signal is a square wave (50% duty cycle).

power in R_o, is

$$R_{ac} = \frac{R_o}{\sqrt{2}}. \tag{14}$$

When S is closed, as current flows through the least resistive path as shown by the dashed line in Fig. 2(a), diodes D_1 and D_2 are virtually out of the circuit. The effective power recovery circuit can be drawn as Fig. 2(b). C_4 and D_3 form a voltage clamp. The equivalent ac load resistance is given by [11]

$$R_{ac} = \frac{R_o}{8}. \tag{15}$$

Because the R_{ac} values given by (14) and (15) differ by a factor of more than five, switching between the two R_{ac}'s will effect a sufficiently large change in the impedance reflected onto the primary coil, hence a high modulation index to support LSK.

With proper circuit design, both η and V_o can be maintained within acceptable limits as R_{ac} changes [3]. At resonance, the power transfer efficiency for both circuit configurations is [11]

$$\eta = \frac{P_o}{P_i} = \left(\frac{R_L}{R_L + R_2}\right)\left(\frac{R_r}{R_r + R_1}\right) = \frac{k^2 Q_1 Q_2^3 R_2 R_{ac}}{(R_{ac} + Q_2^2 R_2)[(1 + k^2 Q_1 Q_2) R_{ac} + Q_2^2 R_2]}. \tag{16}$$

where R_L is the load applied to the secondary coil [11],

$$R_L = \frac{(\omega L_2)^2}{R_{ac}}. \tag{17}$$

P_i is the power output of the RF source and P_o is the power dissipated in R_L. Q_1 and Q_2 are the quality factors for the primary coil and the secondary coil, respectively, R_1 and R_2 are the series resistance values of the primary coil and the secondary coil, respectively, and R_r is the reflected resistance. At resonance, Z_2 is real, so Z_r is purely resistive, hence referred as R_r.

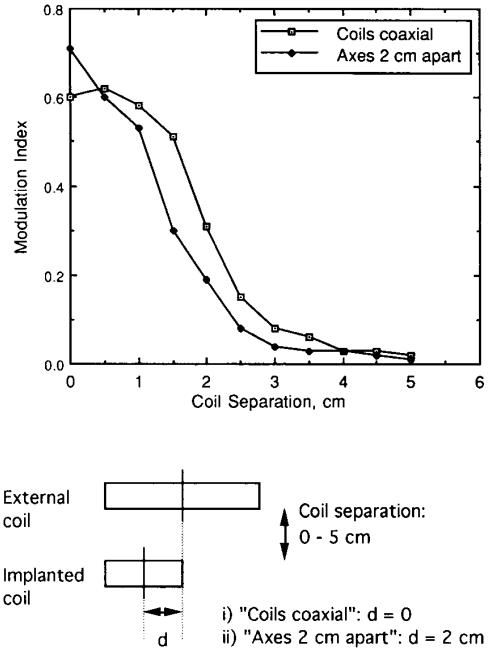

Fig. 5. Modulation index versus coil separation, measured with the circuit in Fig. 4. The demodulation circuits detects signal with modulation index as small as 0.02.

Equation (16) can be rewritten as

$$\eta = \frac{k^2\omega^4 L_1 L_2^3}{\left(R_2 + \frac{\omega^2 L_2^2}{R_{\rm ac}}\right)\left(R_1 R_2 + k^2\omega^2 L_1 L_2 + \frac{R_1\omega^2 L_2^2}{R_{\rm ac}}\right)}. \tag{18}$$

Theoretically, if $\partial\eta/\partial R_{\rm ac} = 0$, then η is independent of $R_{\rm ac}$, and therefore unaffected by load shifting. Unfortunately, the solution of R_2 or $R_{\rm ac}$ for $\partial\eta/\partial R_{\rm ac} = 0$ is negative, and that is not realizable. However, if $R_2 \gg \omega^2 L_2^2/R_{\rm ac}$, then the effect of $R_{\rm ac}$ in (18) is minimized. This implies that both R_2 and $R_{\rm ac}$ should be large to result in a relatively load-independent efficiency. But on the other hand, a large R_2 leads to reduced efficiency. Experiments showed that as a compromise, R_2 could be as small as possible while $R_{\rm ac}$ should be large to result in a relatively high and stable efficiency. By choosing different wire gauges and materials for coil fabrication, R_2 and therefore Q_2 can be changed without significantly changing L_2.

The principle of CCM was verified using SPICE simulation and by experimental measurements.

III. Circuit Implementation

Fig. 3 illustrates an actual LSK-CCM circuit. The carrier frequency was chosen as 8.75 MHz because it satisfies the data communication requirements, while the tissue absorption of electromagnetic energy, which increases with frequency [4], [6], remains insignificant.

The RF coil design procedures introduced by Ko *et al.* [11] and Donaldson *et al.* [3] were used to calculate the number of turns of coils. Titanium wire was chosen for winding the secondary coil based on a compromise among electrical properties, mechanical properties, electrochemical corrosion resistance, and biocompatibility [15].

The circuit configuration switch is a DMOS (Double-diffusion MOSFET) transistor, SD210, manufactured by Siliconix. It meets our requirement of passing 10 mA of current while withstanding 15 V of voltage across it. SD210 conducts in both directions (drain to source and source to drain) when turned on. With $C_{\rm DS} = 2$ pF and $r_{\rm DS} < 100\ \Omega$, it is experimentally proven to be capable of transmitting a 300-kHz square wave. A single CMOS inverter is used as the MOSFET driver, which boosts the logical levels "1" and "0" to voltage levels near V_+ and V_-, respectively. Knowing that the turn-on voltage threshold is appropriate, the increase in driving voltage, V_{GS}, increases the ratio of off-resistance to on-resistance, $r_{\rm DS(off)}/r_{\rm DS(on)}$, hence higher modulation index.

The demodulator can be any envelope detector, which is almost universally used in AM demodulation [14]. The circuit we used is able to detect an AM waveform with a minimum modulation index of about 0.02.

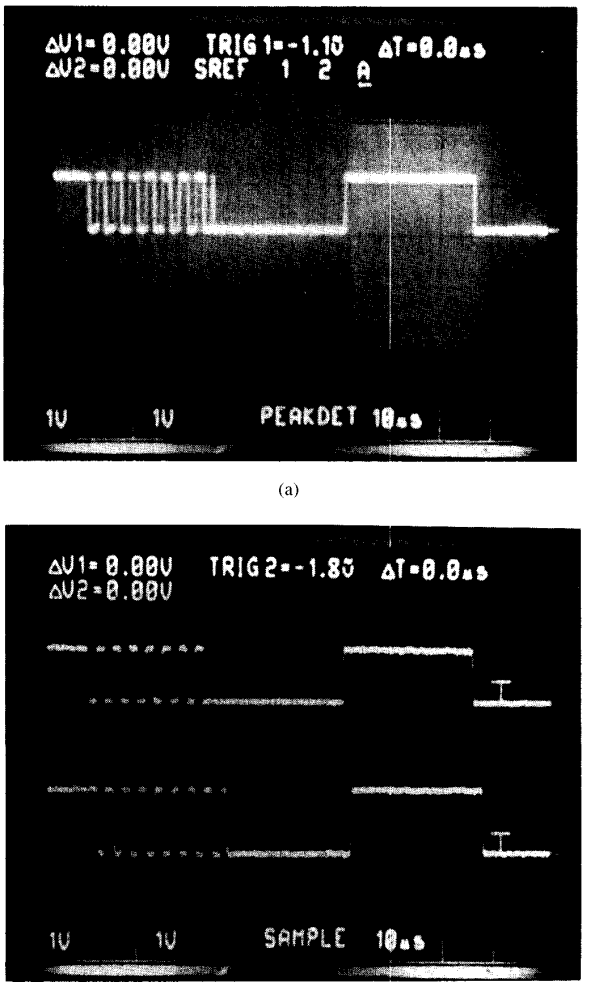

Fig. 6. The oscilloscope view of the data transmission. The data has a speed of 36 kb/s and includes synchronization bursts of 300 kHz. (a) The signal being transmitted and the modulated RF waveform. (b) The upper trace is the signal being transmitted and the lower trace is the signal received.

IV. Evaluation

The circuit shown in Fig. 3 was used for evaluation purposes. The modulation index and power efficiency were measured against coil separations.

Fig. 4 shows the experimental results of power transfer efficiency versus coil separation. The coils were designed and tuned for 2.54 cm (1 in) separation. The power transfer efficiency varied little when the two coils were 100% overlapped (as defined in Fig. 4), regardless of relative movements. The effect of modulation on power transfer efficiency was measured using a square wave data signal at various frequencies. The data frequency had little effect on the power transfer efficiency.

Fig. 5 shows modulation index versus coil separation. The demodulator detected signals having a modulation index as low as 0.02. The measurement was performed using a square wave of 18 kHz representing the data 0101 0101 $\cdots$ at 36 kb/s and of 300 kHz representing a synchronization burst. The data frequency had little effect on the modulation index until it exceeded the limit that the modulation switch (SD210) could handle.

The angle between two coil planes did not significantly affect either power transmission or data transmission as long as it was within $\pm$ 60°.

Fig. 6 shows an oscilloscope view of the actual data being transmitted and the same data being received and demodulated externally.

V. Conclusion

If the lowest acceptable power transfer efficiency is generally defined as 20% and the lowest detectable modulation index is 0.025, the useable range for the tested circuit is about 1–3 cm when the implanted (secondary) coil and the external (primary) coil are 100% overlapped. In our four-channel implantable EMG telemetry system using LSK-CCM [15], the RF powering system transmits the required 80 mW of power when the two coils were separated by less than 3.5 cm, while the distance between the coil axes was less than 2 cm and the angle between the two coil planes was less than 60°. The data transmission link always worked properly within the range in which the powering system worked properly. This is sufficient for our clinical applications. The overall performance can be further improved if the power requirement is made lower. Furthermore, the overall power efficiency is significantly affected by the design of the tuning and impedance matching networks in the transmitting coil with a flexible cable. Our more recent work has indicated that the efficiency given in Fig. 4 could still be significantly increased with further circuit design efforts.

The choice of modulation scheme and modulator depends on if and how they fit into specific device requirements. None of the existing methods should be considered as universally the best. LSK-CCM provides a new alternative for implementing short-range digital AM communication, particularly useful in implantable biotelemetry. For our telemeter design, LSK-CCM means physically the simplest circuit compared to any other existing modulator configurations that we have investigated, including the ones required for FSK and PSK, as well as other ASK implementations. Recently, this technology has also been applied in a multichannel implantable FES system performing bidirectional digital data communications at 5 μs/b while delivering 160 mW of power into the implant with a single RF inductive couple.

References

[1] N. C. Besseling, D. C. van Maaren, and Y. J. Kingma, "An implantable biotelemetry transmitter for six differential signals," *Med. Biol. Eng.*, pp. 660–664, Nov. 1976.

[2] O. Y. De Vel, "Controlled transcutaneous powering of a chronically implanted telemetry device," *Biotelemetry Patient Monit.*, vol. 6, pp. 176–185, 1979.

[3] N. de N. Donaldson and T. A. Perkins, "Analysis of resonant coupled coils in the design of radio frequency transcutaneous links," *Med. Biol. Eng. Comput.*, vol. 21, pp. 612–627, 1983.

[4] O. P. Gandhi, Ed., *Biological Effects and Medical Applications of Electromagnetic Energy*. Englewood Cliffs, NJ: Prentice-Hall, 1990.

[5] B. Hansen, K. Aabo, and J. Bojsen, "An implantable, externally powered radiotelemetric system for long-term ECG and heart-rate monitoring," *Biotelemetry Patient Monit.*, vol. 9, pp. 227–237, 1982.

[6] F. Hochmair, "System optimization for improved accuracy in transcutaneous signal and power transmission," *IEEE Trans. Biomed. Eng.*, vol. BME-31, no. 2, pp. 177–186, 1984.

[7] D. C. Jeutter and E. Fromm, "A modular expandable implantable temprature biotelemeter," *IEEE Trans. Biomed. Eng.*, vol. BME-27, no. 5, pp. 242–247, 1980.

[8] R. Kadefors, "Controlled external powering of miniaturized chronically implanted biotelemetry devices," *IEEE Trans. Biomed. Eng.*, vol. BME-23, no. 2, pp. 124–129, 1976.

[9] H. P. Kimmich, "Biotelemtry," in *Encyclopedia of Medical Devices and Instrumentation*, J. G. Webster, Ed. New York: Wiley, 1988, vol. 1, pp. 409–425.

[10] W. H. Ko, J. Hynecek, and J. Homa, "Single frequency RF powered ECG telemetry system," *IEEE Trans. Biomed. Eng.*, vol. BME-26, no. 2, pp. 105–109, 1979.

[11] W. H. Ko, S. P. Liang, and C. D. Fung, "Design of radio-frequency powered coils for implant instruments," *Med. Biol. Eng. Comput.*, vol. 15, pp. 634–640, 1977.

[12] J. D. Pauley and M. Reite, "A microminiature hybrid multichannel implantable biotelemetry system," *Biotelemetry Patient Monit.*, vol. 8, pp. 163–172, 1981.

[13] J. H. Schild, "A multichannel implantable telemeter for acquisition of physiological data," M.S. thesis, Case Western Reserve Univ., Cleveland, OH, 1988.

[14] F. G. Stremler, *Introduction to Communication Systems*, 2nd ed. Reading, MA: Addison-Wesley, 1982.

[15] Z. Tang, "An implantable multichannel biotelemeter for electromyographic data acquisition," M.S. thesis, Case Western Reserve Univ., Cleveland, OH, 1990.

[16] F. E. Terman, *Radio Engineer's Handbook*. New York: McGraw-Hill, 1943.

[17] B. C. Towe, "Passive biotelemetry by frequency keying," *IEEE Trans. Biomed. Eng.*, vol. BME-33, no. 10, pp. 905–909, 1986.

[18] T. G. Wolcott, "Heart rate telemetry using micropower integrated circuits," in *A Handbook on Biotelemetry and Radio Tracking*, C. J. Amlaner, Jr. and D. W. MacDonald, Eds. New York: Pergamon Press, 1979, pp. 279–286.